Downloaded from https://www.cambridge.org/core. Open University Library, on 22 Jan 2020 at 22:43:52, subject to the Cambridge Core terms of use, available at https://www.cambridge.org/core/terms. https://doi.org/10.1017/jfm.2014.3

J. Fluid Mech. (2014), *vol.* 742, *pp* 291–307. © Cambridge University Press 2014
The online version of this article is published within an Open Access environment subject to the conditions of the Creative Commons Attribution licence <http://creativecommons.org/licenses/by/3.0/>.
doi:10.1017/jfm.2014.3

Velocity–vorticity correlation structure in turbulent channel flow

Jun Chen[1], **Fazle Hussain**[2], **Jie Pei**[1] **and Zhen-Su She**[1,†]

[1]State Key Laboratory for Turbulence and Complex Systems, Department of Mechanics and Engineering Science, College of Engineering, Peking University, Beijing 100871, China

[2]Texas Tech University, Department of Mechanical Engineering, Box 41021, Lubbock, TX 79409-1021, USA

(Received 3 May 2013; revised 16 December 2013; accepted 26 December 2013; first published online 24 February 2014)

A new statistical coherent structure (CS), the velocity–vorticity correlation structure (VVCS), using the two-point cross-correlation coefficient R_{ij} of velocity and vorticity components, u_i and ω_j $(i, j = 1, 2, 3)$, is proposed as a useful descriptor of CS. For turbulent channel flow with the wall-normal direction y, a VVCS study consists of using u_i at a fixed reference location y_r, and using $|R_{ij}(y_r; x, y, z)| \geqslant R_0$ to define a topologically invariant high-correlation region, called $VVCS_{ij}$. The method is applied to direct numerical simulation (DNS) data, and it is shown that the $VVCS_{ij}$ qualitatively and quantitatively captures all known geometrical features of near-wall CS, including spanwise spacing, streamwise length and inclination angle of the quasi-streamwise vortices and streaks. A distinct feature of the VVCS is that its geometry continuously varies with y_r. A topological change of $VVCS_{11}$ from *quadrupole* (for smaller y_r) to *dipole* (for larger y_r) occurs at $y_r^+ = 110$, giving a geometrical interpretation of the multilayer nature of wall-bounded turbulent shear flows. In conclusion, the VVCS provides a new robust method to quantify CS in wall-bounded flows, and is particularly suitable for extracting statistical geometrical measures using two-point simultaneous data from hotwire, particle image velocimetry/laser Doppler anemometry measurements or DNS/large eddy simulation data.

Key words: Boundary layer structure, Turbulent boundary layers

1. Introduction

The concept of coherent structure (CS) is now widely accepted and plays a central role in the dynamical study of turbulent shear flows. Techniques to extract CS features include conditional sampling (Antonia 1981), pattern recognition (Eckelmann *et al.* 1977), proper orthogonal decomposition (POD) (Berkooz *et al.* 1993), eduction of vorticity-based CS (Hussain & Hayakawa 1987; Jeong *et al.* 1997), quadrant splitting methods (Wallace, Eckelmann & Brodkey 1972; Willmarth & Lu 1972; Yang & Jiang 2012) and stochastic estimation (Adrian & Moin 1988). The conditional sampling methods are based on a one-fixed-point scheme typically using streamwise velocity or Reynolds stress $\langle u_1 u_2 \rangle$ as the detection signal (Wallace 2009). A technical difficulty

† Email address for correspondence: she@pku.edu.cn

comes from phase jitter due to the random occurrence, shape, size and orientation of the structures in space and time (Antonia 1981); often the method is applied at several locations to capture different parts of a CS in turbulent boundary layers (TBLs) (Huang *et al.* 2007), with great sophistication (Lo *et al.* 2000). Also, an empirical, and arguable subjective, threshold is inherently needed for defining the boundaries of CS. A recent method identifies Lagrangian coherent structures (LCS) (Shadden *et al.* 2006), which seems to be more 'objective' than Eulerian-based schemes, but requires substantially higher temporal resolution (Pan *et al.* 2009).

The scale of CS has been an important issue in wall-bounded turbulence. In the 1960s, Kline *et al.* (1967) first reported a spanwise scale, $\lambda^+ 100 \sim 100$, for low-speed streaks in TBLs, but later numerical and experimental studies (Smith & Metzler 1983; Kim *et al.* 1987) reveal a linear growth of the spanwise scale of streaks with the distance from the wall. Increasing λ^+ with increasing y is not surprising as the streaks are of varying height. Tomkins & Adrian (2003) asserted that it is consistent with the idea of self-similar growth of structures in an average sense. However, these studies are restricted to CS near the wall. Smith & Metzler (1983) remark that the structures above the buffer layer ($y^+ > 30$) become so complex with distance from the wall that quantifying streak spacing, merging or divisions become too subjective. Thus, it is important to develop new methods for the extraction of the structures in log and outer layers, which are more complicated.

Despite numerous efforts, there are still two additional outstanding issues in CS studies. One is the difficulty in obtaining quantitative measures in a variety of wall-bounded flows, which require a large set of instantaneous flow fields, and the other is incorporation of the CS in engineering models. We focus here on the first issue. Traditional CS studies define the CS from instantaneous flow fields, and obtain statistical measures later. Here, we are motivated to introduce a new concept of CS which is directly related to statistical measures. The new concept is methodologically stable, and easier to carry out throughout the flow domain beyond the near-wall region. The new concept is a statistical CS – the velocity–vorticity correlation structure (VVCS) (Chen *et al.* 2011; Pei *et al.* 2012), using two-point cross-correlation coefficients of the velocity u_i, and vorticity ω_j components ($i, j = 1, 2, 3$). We use channel flow as a platform to illustrate the concept, and the method is equally applicable to other wall-bounded flows, especially TBLs. In this study, u_i is a fixed reference location with a vertical coordinate y_r, while ω_j varies in space of (x, y, z) to form a correlation field. The high-correlation regions (or volumes) defined by the cross-correlation coefficients above a threshold constitute the VVCS. The application of the method to direct numerical simulation (DNS) channel flow data shows that the VVCS qualitatively and quantitatively captures many, if not all, known geometrical features of near-wall CS obtained in prior CS studies, including spanwise spacing, streamwise length and inclination angle of the streamwise vortices and the streaks. The method seems robust and thus provides a new way to quantify CS and hopefully incorporate CS ideas in predictive engineering models.

2. DNS details

DNS data of a fully developed channel flow were used to calculate the correlation coefficients and to provide a quantitative description of the VVCS. The simulation uses a standard spectral method with periodic boundary conditions in the streamwise and spanwise directions. The computation was carried out with over 2 million grid points ($128 \times 129 \times 128$, in x, y and z) for a Reynolds number of 3300, based on

Downloaded from https://www.cambridge.org/core. Open University Library, on 22 Jan 2020 at 22:43:52, subject to the Cambridge Core terms of use, available at https://www.cambridge.org/core/terms. https://doi.org/10.1017/jfm.2014.3

the mean centreline velocity U_c and the channel half-width H, and $Re_\tau \approx 180$ based on the friction velocity u_τ. For the Reynolds number considered here, the streamwise and spanwise computational periods are chosen to be 4π and $4\pi/3$, respectively. The grid spacings in the streamwise and spanwise directions are $\Delta x^+ = 17.7$ and $\Delta z^+ = 5.9$ in wall units, respectively. Non-uniform meshes were used in the normal direction with $y_i = \tanh(B(2i/(N-1)-1))/\tanh(B), \quad i = 0, 1, \ldots, N$. Here $N = 129$ is the number of grid points in the y direction, and $B = 2.0$. The first mesh point near the wall is at $y^+ = 0.05$ (the superscript '+' denotes normalization by u_τ and viscosity ν), and the maximum spacing (at the centreline of the channel) is 4.42 wall units. This resolution is appropriate for this flow (Li *et al.* 2001), with the mean velocity profile shown in figure 1. A log layer ranging from $y^+ \sim 40$ to 150 agrees with the standard computational fluid dynamics (CFD) results of Kim *et al.* (1987) and experiments of Hussain & Reynolds (1975).

Since the VVCS study investigates the structural properties over the entire channel (not restricted to the near wall region), it is important to gain an insight to the energy dynamics throughout the channel. This is revealed by the budget terms in the equation for the plane-averaged turbulence kinetic energy, $\langle k \rangle = \langle u_i u_i/2 \rangle$, written as

$$\frac{\mathrm{D}}{\mathrm{D}t}\langle k \rangle \equiv \left(\frac{\partial}{\partial t} + U\frac{\partial}{\partial x} + V\frac{\partial}{\partial y} + W\frac{\partial}{\partial z} \right) \langle k \rangle = P + T + D + \Pi - \epsilon \tag{2.1}$$

where various terms are

$$P = -\langle u_i u_j \rangle \frac{\partial U_i}{\partial x_j} = -\langle uv \rangle \frac{\partial U}{\partial y}, \tag{2.2a}$$

$$T = -\frac{1}{2}\frac{\partial}{\partial x_j}\langle k u_j \rangle = -\frac{1}{2}\frac{\partial}{\partial y}\langle kv \rangle, \tag{2.2b}$$

$$D = \nu \frac{\partial^2}{\partial x_j \partial x_j}\langle k \rangle = \nu \frac{\partial^2}{\partial y^2}\langle k \rangle, \tag{2.2c}$$

$$\Pi = -\frac{1}{\rho}\frac{\partial}{\partial x_i}\langle u_i p \rangle = -\frac{1}{\rho}\frac{\partial}{\partial y}\langle vp \rangle, \tag{2.2d}$$

$$\epsilon = \nu \left\langle \frac{\partial u_i}{\partial x_j}\frac{\partial u_j}{\partial x_i} \right\rangle. \tag{2.2e}$$

Summation over repeated indices is implied. Normalized by the dissipation in the wall units, u_τ^4/ν, the terms in (2.2) are, respectively, the turbulence production P, the turbulent transport T, the viscous diffusion D, the pressure transport Π and dissipation ϵ. Figure 2 shows the y-dependence of these terms, calculated from the DNS data. The results validate of the computation, as well as a multilayer structure reported recently by She *et al.* (2010) and Wu *et al.* (2012). In particular, there exists a transition from the quasi-balance region (production–dissipation balance) to the central core region (transport–dissipation balance) at $y^+ \sim 125$. The flow in the central core region is nearly homogeneous in the y direction; the VVCS study captures some of these features.

3. Velocity–vorticity correlation structure

We denote the streamwise coordinate, and the velocity and vorticity components as x, u_1 and ω_1; the wall-normal components as y, u_2, ω_2; and the spanwise components

Downloaded from https://www.cambridge.org/core. Open University Library, on 22 Jan 2020 at 22:43:52, subject to the Cambridge Core terms of use, available at https://www.cambridge.org/core/terms. https://doi.org/10.1017/jfm.2014.3

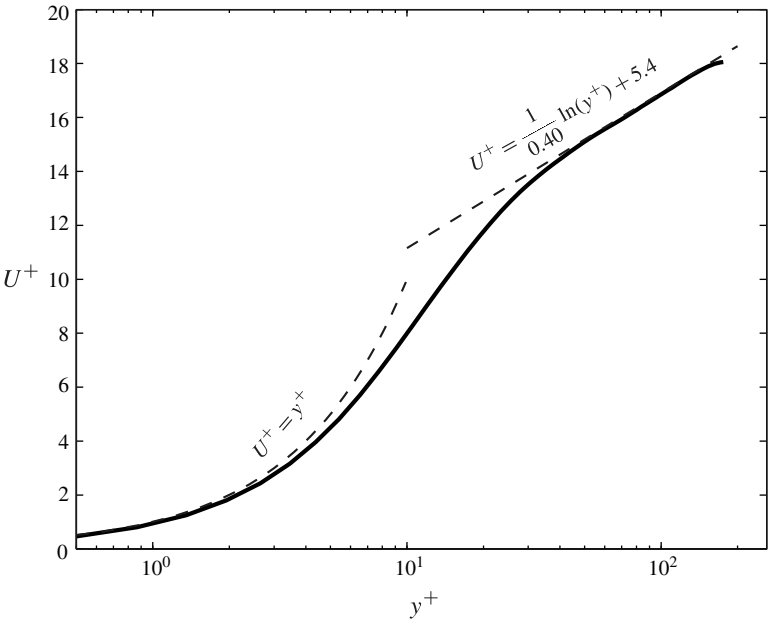

FIGURE 1. Velocity profile in wall units for the present DNS of the channel flow.

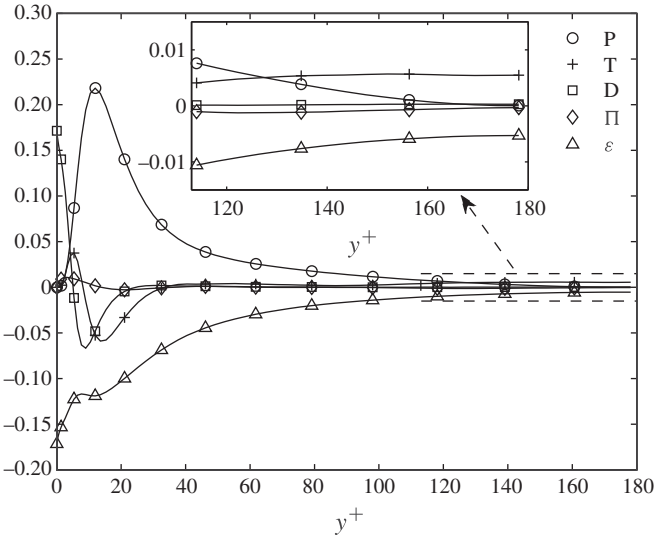

FIGURE 2. The terms in the turbulent kinetic energy budget as a function of y^+, at $Re_\tau = 180$. The inset is the enlarged view of the region marked by rectangle.

as z, u_3, ω_3. The velocity–vorticity correlation coefficient is defined as

$$R_{ij}(x_r, y_r, z_r; x, y, z) = \frac{E\left[(u_i - \overline{u}_i)_A \left(\omega_j - \overline{\omega}_j\right)_B\right]}{u_{i,rms}(y_r) \cdot \omega_{j,rms}(y)}, \tag{3.1}$$

where $A = (x_r, y_r, z_r)$ and $B = (x, y, z)$, denote the reference point for velocity and variable point for the vorticity, respectively, and $i, j = 1, 2, 3$. Here E is the expected

Downloaded from https://www.cambridge.org/core. Open University Library, on 22 Jan 2020 at 22:43:52, subject to the Cambridge Core terms of use, available at https://www.cambridge.org/core/terms. https://doi.org/10.1017/jfm.2014.3

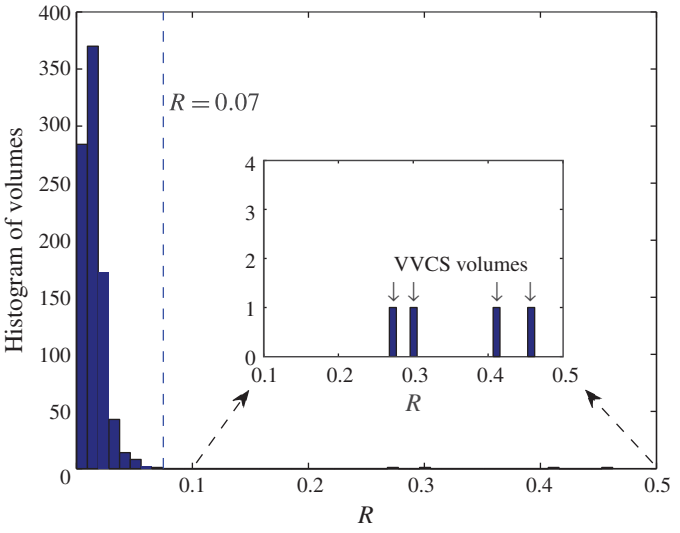

FIGURE 3. (Colour online) Histogram showing the number of volumes binned according to their local peak correlation coefficients. Here $y_r^+ = 3.5$. Four volumes exist for $R \geqslant 0.27$, as shown in the inset.

value. Since fully developed channel flow is homogeneous in the streamwise and spanwise directions, R_{ij} was finally obtained by ensemble averaging the correlation coefficient in these two directions, and is denoted by $R_{ij}(y_r; x, y, z)$.

The computation of the two-point correlation coefficient can be carried out in the whole flow domain. Here R_{ij} varies between -1 and 1, and an isosurface of $R_{ij} = r$, $r \in [-1, 1]$, defines a set of geometrical volumes. For the channel flow data, we calculated the number of the volumes, denoted by $N_v(R)$, as a function of the local peak correlation coefficient $|R_{ij}| = R$, as shown in figure 3. We found that most of the (unconnected) volumes occupy lower correlation coefficient, and when R reaches $R_0 \approx 0.07$, only four volumes with higher correlation coefficient ($R > 0.27$) exist. Thus, for a range of R (between 0.07 and 0.27), we say that the VVCS defines a set of topologically invariant objects – VVCS structures. Topological invariance here means that further raising R within a substantial range does not change the topology, while the isosurfaces under the threshold, R_0, are much more complex (with a large $N_v(R)$). Note that the VVCS structure depends on the reference point location (y_r) and on the components (i and j). The volumes, obtained for velocity u_i and vorticity ω_j and denoted as $VVCS_{ij}$, represent the ω_j regions most correlated to u_i at a specified reference point, say point A.

Careful tests show that $R_0 = 0.07$ is quite universal for all reference locations and for different components of i and j. Hence, we use this empirical value to define the VVCS. In contrast to prior techniques which first identify vortices, and carry out a statistical calculation of the geometry, the VVCS method performs the correlation calculation first. Note that the current VVCS schema can be extended to the two-point correlation of a velocity and a gradient component (or a velocity difference), if the vorticity field is not available. While the VVCS defined above involves several components, the classification of which is an issue to be addressed in the future, we here demonstrate, with application to DNS channel flow data, that it is a useful tool to characterize CS.

Downloaded from https://www.cambridge.org/core. Open University Library, on 22 Jan 2020 at 22:43:52, subject to the Cambridge Core terms of use, available at https://www.cambridge.org/core/terms. https://doi.org/10.1017/jfm.2014.3

It is noteworthy that, by definition, R_{ij} depends on the reference location y_r. Hence, the VVCS defines a family of coherent vortical structures associated with velocity fluctuations with varying y_r. A distinct feature of this family is a discovered topological change in turbulent channel flows, from shear-dominated to central nearly homogeneous regimes, consistent with 'the multilayer picture' proposed recently in a mean-field theory of wall-bounded turbulence (She *et al.* 2010; Wu *et al.* 2012).

4. VVCS in a turbulent channel flow

The $VVCS_{11}$ obtained using the definition introduced above is displayed in figure 4. The $VVCS_{11}$ at small y_r ($y_r^+ < 110$), as shown in figure 4(*a* and *b*), displays two pairs of substructures, both elongated in the x direction. One pair moves with y_r, while the other pair remains attached to the wall. The length of the structures decreases with increasing y_r. For $y_r^+ \geqslant 110$, only one pair of *blob-like* structures close to y_r remain, the near-wall ones having disappeared. Thus, the $VVCS_{11}$ undergoes a change from *four cigar-like (quadrupole) structures* to *two blob-like (dipole) structures* at $y_r^+ \approx 110$. The two topologies of the VVCS are interpreted as different types of vortical motions in turbulence: (*a*) the first type is associated with the shearing turbulence ($y_r^+ < 110$), with one pair of vortices attached to the wall while the other pair remains at comparable height as y_r; (*b*) the second type with a pair of vortical patches (for $y_r^+ > 110$). The topological change of the VVCS will be discussed further below.

We call the pair of $VVCS_{11}$ attached to the wall the *near-wall correlation structures* (NWCS), which have a long streamwise extent and small thickness ($y^+ < 20$). Owing to the wider extent in z than in y, the vertical shear ($\partial w/\partial y$) dominates the spanwise gradient ($\partial v/\partial z$) in ω_1. Hence, the $NWCS_{11}$ is attributed to the effects of the internal shear layers (or vorticity sheets), which is shown to be a fundamental structure below each quasi-streamwise vortex. The streak transient growth (STG) theory suggests that a sheet of streamwise vorticity ω_1 is formed and driven by the combined effect of the streak shear ($\partial U/\partial y$) and the variation of w in the streamwise direction (Schoppa & Hussain 2002). Considering its location and aspect ratio, the $NWCS_{11}$ is believed to be an average of the near-wall vortex which is the ω_1 layer attached to the no-slip wall.

Similarly, we call the upper structure the *accompanying streamwise correlation structure* (ASCS), because this pair follows closely with y_r: as y_r increases, the pair of ASCS are more inclined to the wall, very similar to the conceptual model of counter-rotating streamwise vortices proposed by Townsend (1970). It is interesting to note that, as y_r approaches 0, the ASCS approaches a minimum distance from the wall, which is denoted as $y_{s,0} = \lim_{y_r \to 0} y_s(y_r)$. The definition of y_s (structure location) and y_r (reference location) can be found in figure 5(*a*). For $ASCS_{11}$, $y_{s,0}^+ \approx 17$ coincides with the location of the maximum turbulence production in channel flows (Kim, Kline & Reynolds 1971). Recently, we have shown in compressible channel flow up to Mach number 3 that $y_{s,0}$ defines an important location, where both the mean velocity and root-mean-square (r.m.s.) fluctuation profiles collapse for different Mach numbers (Pei *et al.* 2013). The similarity of the mean velocity profiles in the VVCS-based coordinates, normalized with $y_{s,0}$, has been observed for several Mach number flows, as shown in figure 6. This special VVCS structure at $y_{s,0}$ is called the limiting VVCS structure, whose characteristics are believed to be important for turbulence modelling.

Brooke & Hanratty (1993) in their DNS study of channel flow presented the evidence for quasi-streamwise vortices for $y^+ < 40$, while Christensen & Adrian (2001) suggested that hairpin packets cannot reach more than 100 wall units. We have

Downloaded from https://www.cambridge.org/core. Open University Library, on 22 Jan 2020 at 22:43:52, subject to the Cambridge Core terms of use, available at https://www.cambridge.org/core/terms. https://doi.org/10.1017/jfm.2014.3

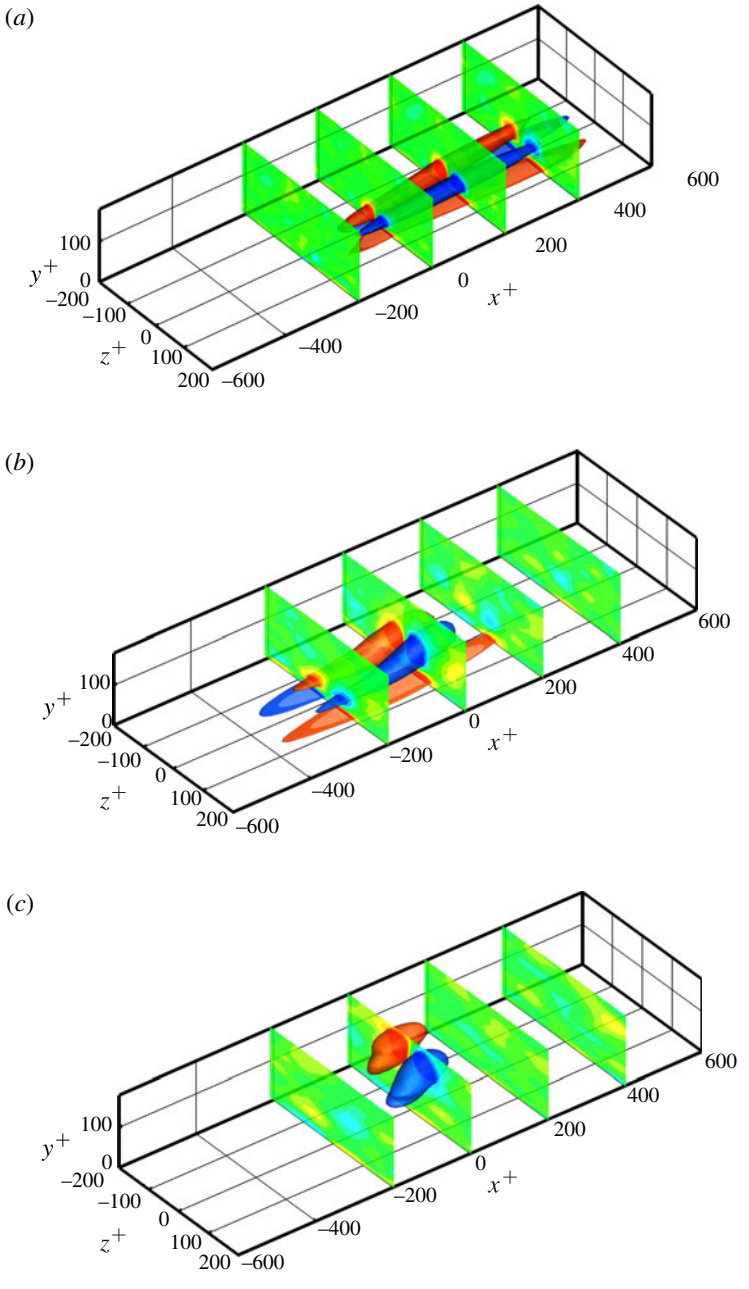

FIGURE 4. The isosurface of the two-point cross-correlation coefficient for R_{11} of an incompressible channel flow for $Re_\tau = 180$. The red surface is defined by the positive threshold of $R_{11} = 0.07$, and the blue surface is defined by the negative threshold of $R_{11} = -0.07$. The slices in the y–z plane show distribution of R_{11} with the spacing of $\Delta x^+ = 200$. The same threshold is used for identifying other VVCS unless mentioned otherwise. Note a topological change from (*a*) and (*b*) (four cigar-like elongated structures) to (*c*) (two blob-like structures): (*a*) $y_r^+ = 3.5$; (*b*) $y_r^+ = 59$; (*c*) $y_r^+ = 145$.

Downloaded from https://www.cambridge.org/core. Open University Library, on 22 Jan 2020 at 22:43:52, subject to the Cambridge Core terms of use, available at https://www.cambridge.org/core/terms. https://doi.org/10.1017/jfm.2014.3

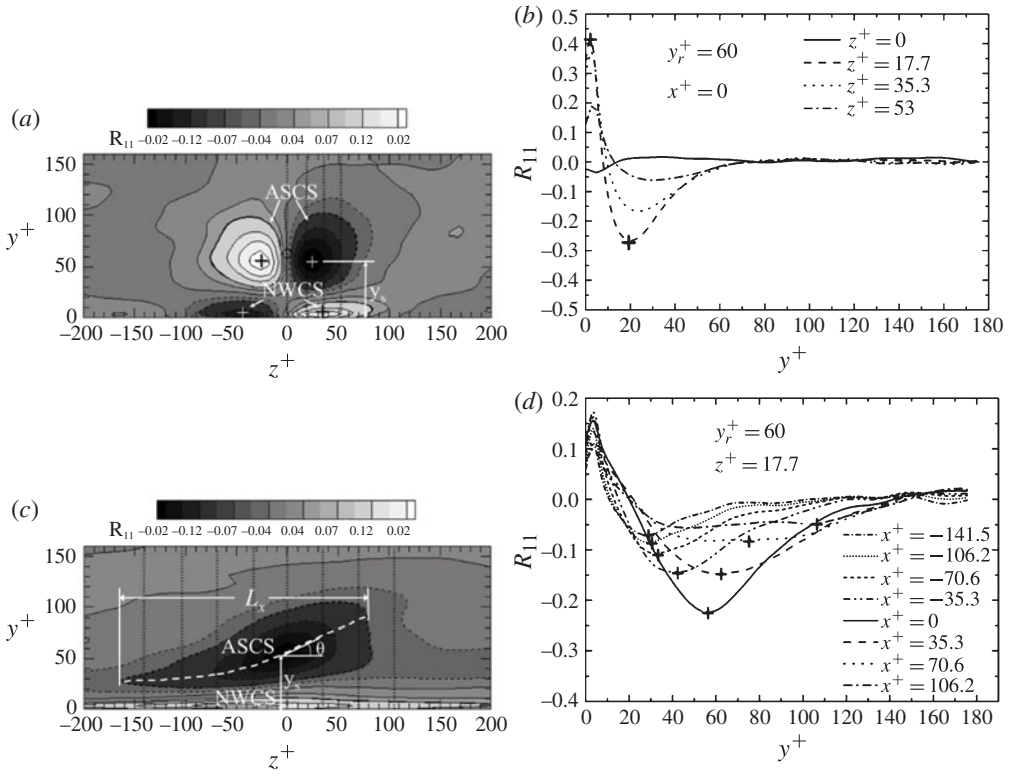

FIGURE 5. (*a*) Contour plot of R_{11} for $y_r^+ = 60$ on the y–z plane at $x^+ = 0$. The white and black '+' represent the positions of the minimum and maximum R_{11}, respectively, marking the centre for each volume. Its vertical coordinate denotes the wall distance y_s of a structure, and the spanwise distance between two centres measures the spanwise spacing D_z. (*b*) Plot of R_{11} versus y^+ at four spanwise locations, marked by vertical dashed lines in (*a*). Here '+' marks the location of the peaks in (*a*) (i.e. the centres of the VVCS). (*c*) Contour plot of R_{11} for $y_r^+ = 60$ on the x–y plane at a typical spanwise location ($z^+ = 17.7$). The white dashed line represents the centreline of the $VVCS_{11}$, defined by a series of (local) peaks found at each fixed streamwise location (such as that shown in *b*), and the length of a VVCS is defined by the centreline in the volume. The inclination angle θ is defined as the tangential angle of the centreline. (*d*) Profiles of R_{11} along marked dashed lines in (*c*). The crosses '+' (shown in red online) mark the position of the most negative correlation coefficients. Note that the thick dashed contours in (*a*) and (*c*) correspond to the isosurfaces (volumes) drawn in figure 4.

a similar finding: a persistence of both NWCS and ASCS for $y_r^+ < 110$ with a disappearance of NWCS at $y_r^+ \sim 110$. Beyond the critical distance from wall (110), only ASCS are present and velocity fluctuations at y_r are correlated only to its nearby blob-like $ASCS_{11}$. A recent mean-field theory (She *et al.* 2010; Wu *et al.* 2012) characterizes this central core region with a transition from the shear-dominated quasi-balance between turbulence production and dissipation to a balance between turbulent transport and dissipation, with a distinct scaling of the mixing length. Considering that the upper bound of the log layer is $y^+ \sim 110$ (as shown in figure 1), we speculate that the transition from quadrupole to dipole is associated with some qualitative change in statistical properties such as the balance mechanism; this transition may

Downloaded from https://www.cambridge.org/core. Open University Library, on 22 Jan 2020 at 22:43:52, subject to the Cambridge Core terms of use, available at https://www.cambridge.org/core/terms. https://doi.org/10.1017/jfm.2014.3

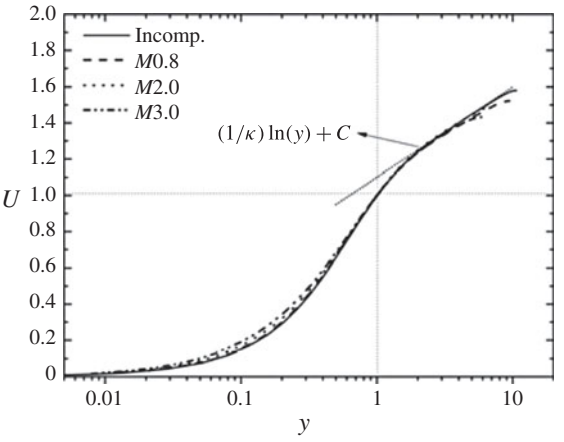

FIGURE 6. The collapse of the rescaled mean velocity profiles using the length scale and the mean velocity of the lowest VVCS in the channel flows at different Mach numbers, $M = 0.8$, 2.0 and 3.0, respectively. (Reproduced with permission from Pei *et al.* (2013, figure 9(*c*)).)

not be thorough at the current moderate Re, but a qualitative feature is discernible. The energy budget in figure 2 supports this speculation with a transition at $y^+ \sim 130$. Hence, the VVCS provides a characterization of the multi-layer statistical structure.

In order to obtain quantitative measures of the $VVCS_{11}$, we try to quantify the contours of $R_{11} = R$. For instance, the contours of $R_{11} = 0.07$ on a y–z plane is shown in figure 5(*a*) for $y_r^+ = 60$ (a typical location in the log region), which clearly establishes four regions with alternate signs of correlations, revealing a quadrupole structure. Detailed variation of R_{11} along the y direction at a few specific spanwise locations are shown in figure 5(*b*): the upper structures are located around the reference location at about $y_s^+ = 42$ with a spanwise spacing of 40, while the lower structures sit always around $y_s^+ = 3 \sim 5$ with a wider spanwise spacing of 60.

The ensemble-averaged λ_2 structures (Jeong & Hussain 1995) suggested that instantaneous near-wall vortices inherently overlap and stagger (Schoppa & Hussain 2002) rather than being side-by-side aligned, suggested by many. However, the long-time ensemble average over many structures will produce side-by-side statistical structures, which correspond to the present observations. The spanwise tilt reported by Jeong *et al.* (1997) is not seen here as they distinguished $+\omega_1$ from $-\omega_1$. We believe that a subensemble calculation involving only $+\omega_1$ (or $-\omega_1$) will capture the tilt as well, which will be studied in the future.

One important quantitative feature of the VVCS is the inclination angle of the ASCS, called θ, defined in the caption of figure 5. The results show that $\theta_{max} \approx 13^\circ \sim 14^\circ$, occurring at $y_s^+ \approx 70$ for $ASCS_{11}$, separating a near-wall region of increasing θ from a bulk flow region where θ decreases with y_s, as shown in figure 7. These angles agree well with the experimental observations from the space-time correlation calculations by Rajagopalan & Antonia (1979), who claimed that the inclination angle of the near-wall large organized structure is 4°. The oblique angles of $ASCS_{11}$ and $ASCS_{12}$ near the wall, $\theta \sim 4^\circ$, are similar to the angle between the high-speed fluid fronts and the wall, 4.7°, as measured by Kreplin & Eckelmann (1979). This angle approaches a maximum of 14° when moving away from the wall. Other observations by Adrian, Meinhart & Tomkins (2000) and Christensen & Adrian

Downloaded from https://www.cambridge.org/core. Open University Library, on 22 Jan 2020 at 22:43:52, subject to the Cambridge Core terms of use, available at https://www.cambridge.org/core/terms. https://doi.org/10.1017/jfm.2014.3

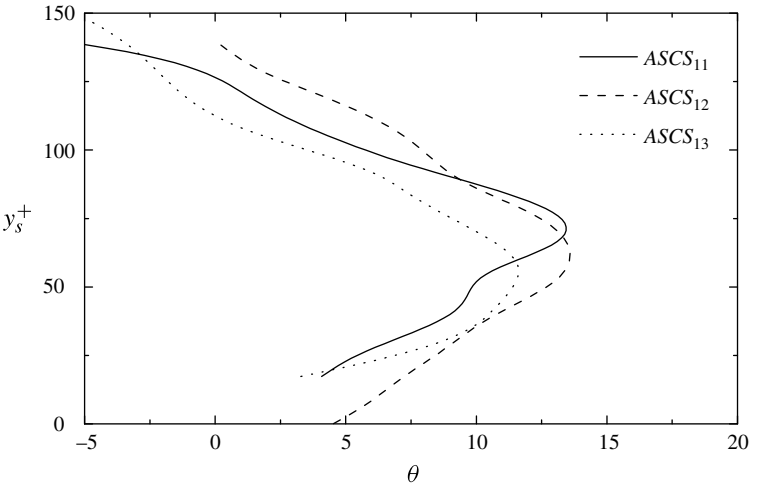

FIGURE 7. The inclination angle, θ, for $ASCS_{ij}$.

(2001), concerning packets of hairpin structures, seem to show similar angles: $\theta \sim 12°$. Recent experimental study in supersonic TBL suggests that the inclination angle of the CS in the near-wall region ($y^+ \leqslant 30$) ranges from 5° to 15° (He *et al.* 2011), similar to our observations.

It is noteworthy that the inclination angle of $ASCS_{11}$ at $y_s^+ = 20$ is ~4° (see figure 7), smaller than 9° obtained from an ensemble study of λ_2 structures (Jeong *et al.* 1997). This is because the ASCS structures capture more near-wall quasi-streamwise vortices, e.g. the legs of the hairpins ($y^+ \leqslant 15$), which have smaller inclination angles (Adrian *et al.* 2000) in comparison with Jeong's observation; the latter concerns the quasi-streamwise vortices generated around $y^+ \sim 20$. The agreement between the present VVCS study at moderate *Re* and previous measurements at high *Re* suggests that the VVCS are independent of *Re*.

Figure 8 reports the profile of D_z^+ which increases linearly with y_s^+ over most parts of the domain, with a good collapse as (D_z^+ is defined in figure 5):

$$D_z^+ = 0.31 y_s^+ + 30.3. \tag{4.1}$$

Note that the linear profile extends up to $y_s^+ = 140$, far beyond the range in previous experimental studies of CS. This result suggests that coherence extends even to the centre of channel with well-developed turbulence. It is noteworthy that linear increase of the spanwise spacing is also observed for $NWCS_{11}$, as shown in figure 9.

The length scale of $ASCS_{11}$, shown in figure 10, decreases with increasing y_s, consistent with a more homogeneous and isotropic flow and with a transition from a shear-dominated energy budget to a turbulent transport-dominated energy budget, as discussed in § 2. Previous studies using Fourier transform or two-point autocorrelation of the velocities, yield also a distribution of scales, but did not give the geometry (e.g. shape) of the structure, especially near the central region (Krogstad & Antonia 1994; Flores & Jiménez 2006). The VVCS has an advantage in this regard. The present study has provided a quantitative characterization of the vortical structures in the region beyond the log layer. This success of defining the geometrical measures ($L_x^+ \approx 100$) in the central region is due to the VVCS's definition. Of course, for an

Downloaded from https://www.cambridge.org/core. Open University Library, on 22 Jan 2020 at 22:43:52, subject to the Cambridge Core terms of use, available at https://www.cambridge.org/core/terms. https://doi.org/10.1017/jfm.2014.3

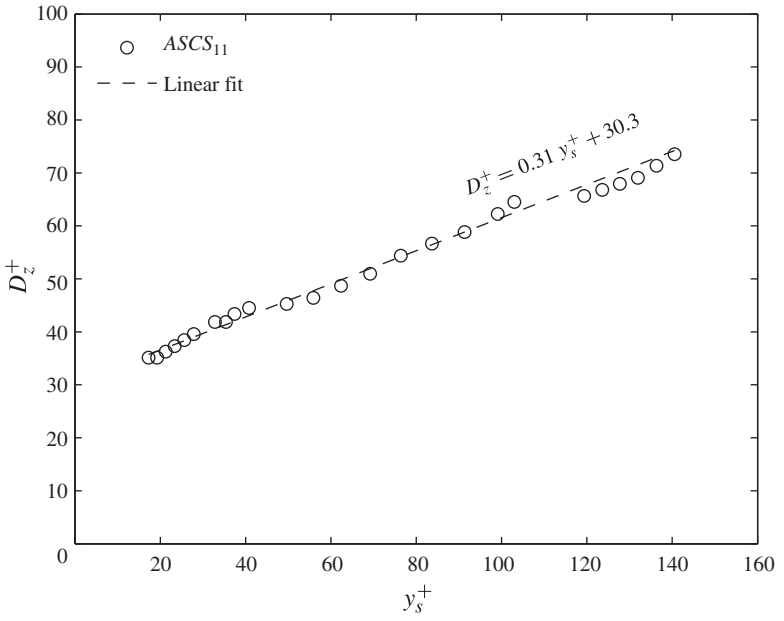

FIGURE 8. The spanwise distance, D_z, of $ASCS_{11}$. The dashed line is the linear fit of the profiles.

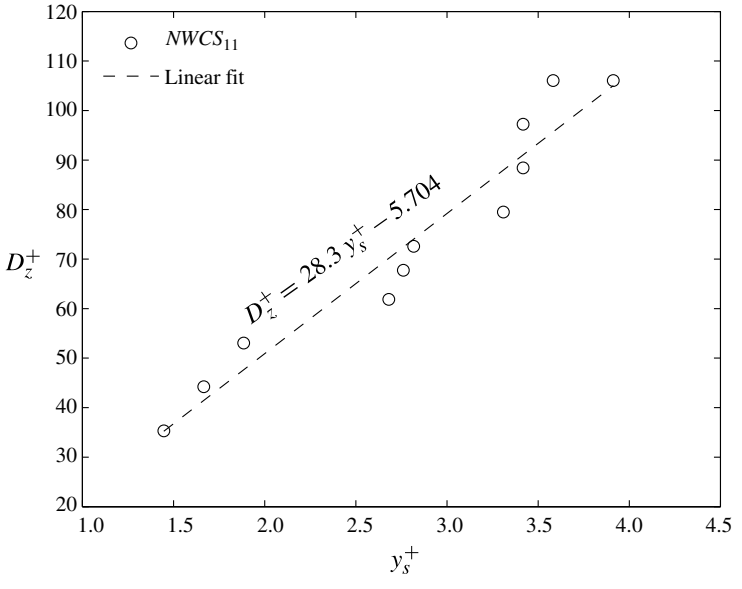

FIGURE 9. The spanwise distance, D_z, of $NWCS_{11}$. The dashed line is the linear fit of the profiles.

ideally homogeneous and isotropic turbulence in a periodic box, the VVCS measures should be zero. Thus, the non-zero VVCS structure around the centreline of a

Downloaded from https://www.cambridge.org/core. Open University Library, on 22 Jan 2020 at 22:43:52, subject to the Cambridge Core terms of use, available at https://www.cambridge.org/core/terms. https://doi.org/10.1017/jfm.2014.3

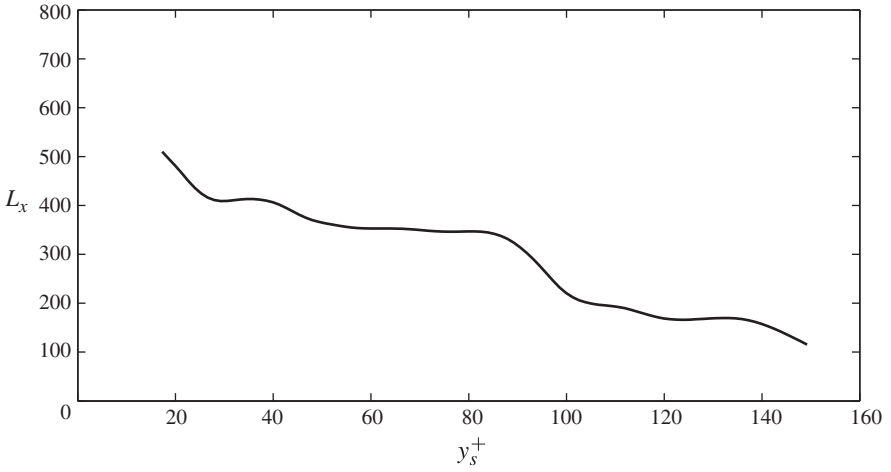

FIGURE 10. The length, L_x, of $ASCS_{11}$.

channel is non-trivial, and the connection between the shape of the blob and the energy/momentum transfer would be an intriguing topic for future study.

Note that the study of $VVCS_{11}$ has successfully established a prediction model of the whole profile of the propagation speed in the compressible turbulent channel flow (Pei *et al.* 2012). It is expected to yield in the future other quantitative models for the statistical quantities.

The three-dimensional structure of $VVCS_{13}$ is shown in figure 11. Here $VVCS_{13}$ is a long streamwise vortical structure parallel to the wall at the centreline with three opposite-signed vortical structures around it. Klewicki & Falco (1996) identified the ω_3-eddies by measuring $\langle\omega_3\omega_3\rangle$ with two hot-wire probes separated in the spanwise as well as the wall-normal directions, which show similar structures as ours.

Another interesting result is the topological variation of $VVCS_{13}$ with y_r, as shown in figure 11. Note that the principal feature of the $VVCS_{13}$ consists in one $ASCS_{13}$ (upper part) and three $NWCS_{13}$ (lower part) at small y_r, which transform to a pair of vertically aligned $ASCS_{13}$ in the interval of $y_r^+ \approx 40 \sim 60$. A further transformation takes place at $y_r^+ \geqslant 100$, with a single $NWCS_{13}$ attached to the wall. This topological change illustrates an important difference between the near-wall region CS and log-layer CS; the latter is characterized by two cigar-like elongated structures shown in figure 11(*c*). Although more extensive study is needed to confirm this observation in the future, let us note a consistent experimental observation of Klewicki, Murray & Falco (1994): one $+\omega_3$ eddy above the probe and another $-\omega_3$ one below the probe. Note that the $NWCS_{13}$ always exists, even for $y_r^+ > 100$, indicating that u_1' over the whole domain affects $\partial u_1/\partial y$ near the wall.

The topological variation of the $VVCS_{13}$ is also consistent with the measurements of instantaneous structures. Zhou *et al.* (1999) asserted that the instantaneous quasi-streamwise vortices, in terms of the legs of hairpins, mainly exist below $y^+ \sim 100$ (corresponding to the quadrupole structures of $ASCS_{11}$) and the heads of the hairpins (interpreted as the blob-like structures of $ASCS_{13}$) may reach up over $y^+ \sim 200$.

Considering the two separated structures of $-\omega_3$ for larger y_r, the streamwise velocity u_1' is driven by both the accompanying vorticity structure right below y_r as well as the near-wall attached structure, as shown in figure 11(*b*, *c*). Far away from the wall, the blob-like $ASCS_{13}$ are also observed for $y_r^+ > 80$, as seen in figure 11(*c*),

Downloaded from https://www.cambridge.org/core. Open University Library, on 22 Jan 2020 at 22:43:52, subject to the Cambridge Core terms of use, available at https://www.cambridge.org/core/terms. https://doi.org/10.1017/jfm.2014.3

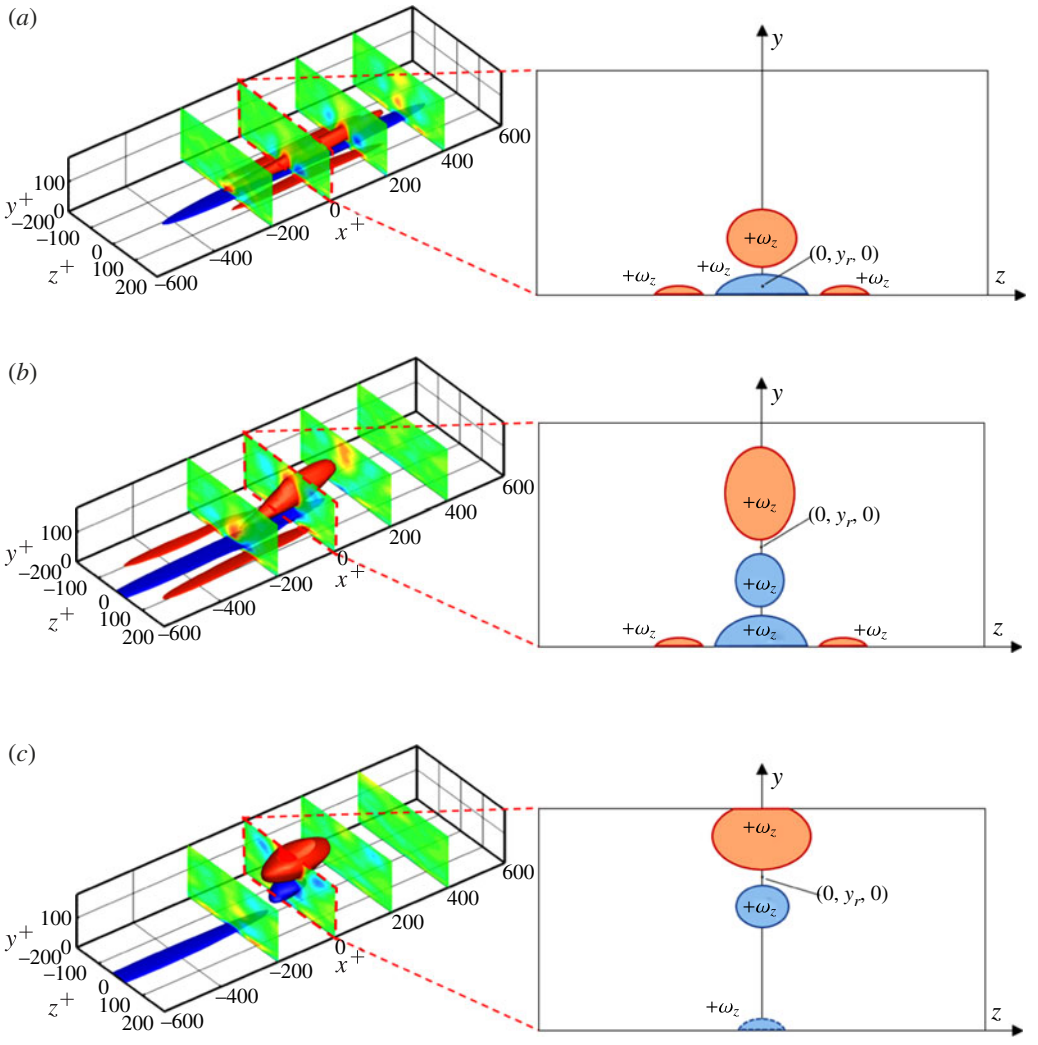

FIGURE 11. Left: Isosurface of the two-point cross-correlation coefficient R_{13}. The cross-sections show distribution of the correlation coefficient on y–z plane with the spacing of $\Delta x^+ = 200$. Right: Schematics of the volume of $VVCS_{13}$ corresponding to the cross-section at $x = 0$, marked by the red dashed frame in the coefficient field: (*a*) $y_r^+ = 3.5$; (*b*) $y_r^+ = 59$; (*c*) $y_r^+ = 120$.

indicating that turbulence is statistically nearly homogeneous in the central region. In particular, the vertically-aligned pair of blob-like structures have more vertical extent, distinct from horizontally extended $ASCS_{11}$.

5. Conclusion and remarks

The VVCS, using two-point cross-correlation coefficients of the velocity u_i and the vorticity ω_j components, reveals two important features of CS: first, there exists a family of structures, each influencing velocity fluctuations at any reference point (denoted as y_r); and, second, the geometry of different vorticity components exhibiting

Downloaded from https://www.cambridge.org/core. Open University Library, on 22 Jan 2020 at 22:43:52, subject to the Cambridge Core terms of use, available at https://www.cambridge.org/core/terms. https://doi.org/10.1017/jfm.2014.3

a rich set of behaviors. The features captured in the present study are qualitatively and quantitatively consistent with those obtained in the previous CS studies, as summarized in table 1. In addition, the variation of VVCS with y_r provides a proof of the existence of the central core layer (She *et al.* 2010; Wu *et al.* 2012). Hence, a complete geometrical description of wall-bounded turbulence requires a series of VVCS (with varying y_r). Since different shears produce different sets of geometrical structures, as displayed by VVCS, a multilayer structure is necessary for describing the wall-bounded turbulence (She *et al.* 2010; Wu *et al.* 2012). Furthermore, VVCS provides an effective method to quantify CS over the whole flow domain, which is believed to be important in turbulence modelling.

A fundamental difference between prior CS calculation and the VVCS method is that the former characterizes the geometry of an instantaneous full velocity gradient field, but the latter quantifies the correlation field. The spatial distribution of the two-point correlation coefficients can be obtained by moving pairs of hotwire probes, in the absence of a full velocity field. In fact, the conventional definition of CS and the VVCS are two sides of a coin: the former extracts the statistical measures from the geometry of instantaneous fields, while the latter displays geometrical features of turbulent structures directly from statistical correlation measures. VVCS captures well quantitative measures such as width, length, spacing and inclination angle, and reveals that statistics and geometry are intimately related. One might continue to wonder whether VVCS capture 'real' structures; we suggest to leave this problem but focus on a more intriguing question: how are the measured quantities relevant to turbulence modelling? This last question is one of the most challenging in the CS study. We hope to have moved one step further in this direction, as we have at least inferred features of turbulent structures directly from the statistical measures: two-point correlation coefficients. The VVCS identified in the present study describes a region (volume) of the vorticity fluctuations most correlated to velocity fluctuations at a (fixed) location (y_r). Since this volume is defined in terms of the vorticity, we also call it a 'vortical' structure.

In this paper, we have mainly established the validity of the concepts; the study of *Re* effects will be reported elsewhere. One might question whether the simulation data has a too low *Re*; we believe not. Low *Re* effects have been extensively investigated in the past; Antonia & Kim (1994) reported that despite the growth of the vorticity, dissipation and Reynolds stress with *Re*, the geometrical measures (diameter and the location) of the quasi-streamwise vortices do not change. On the other hand, even at a very moderate *Re*, the statistical multilayer structure of a fully developed turbulence has completely formed, including the viscous sublayer, the buffer layer, the log bulk layer and the central core region (She *et al.* 2010; Wu *et al.* 2012). Figure 1 shows that $3/4$ of the channel is occupied by turbulence characteristic of the log region and central core region. Whether the results presented here are relevant to higher *Re* is an open question. A positive answer is provided by quantitative agreement of the measured VVCS characteristics of the structures (width, length and inclination angle) with experimental measurements, and a firm answer can only be obtained by extending the analysis to other higher *Re* data in the future.

Finally, the concept of the VVCS can be generalized to other variables different from the velocity and vorticity. Examples include velocity-density correlation structure, velocity-temperature correlation structure, velocity-pressure correlation structure in compressible flows. Such studies should reveal new features and new interpretations enriching the notion of turbulent structures.

Downloaded from https://www.cambridge.org/core. Open University Library, on 22 Jan 2020 at 22:43:52, subject to the Cambridge Core terms of use, available at https://www.cambridge.org/core/terms. https://doi.org/10.1017/jfm.2014.3

Coherent structures	Quantitative measures of CS	Corresponding features of VVCS
Streamwise vortices and large-scale structures	The inclination angle starts with 4°, and approaches its maxima of 14° with increasing wall distance (Rajagopalan & Antonia 1979).	The inclination angle of $ASCS_{11}$ and $ASCS_{13}$ increase from 4° to 14° while y_s^+ increases from 0 to 70 (figure 7).
	The ensemble-averaged CS are inclined 9° in the x–y plane (Jeong *et al.* 1997).	The inclined angle $ASCS_{11}$ at $y_r^+ = 40$ is ∼9° (figure 7).
	Streamwise extent of two x-displaced counter-rotating adjacent coherent structures educed from near-wall turbulence is 320 wall units (Jeong *et al.* 1997).	The length of $ASCS_{11}$ decreases from 500 to 300 when for y_s^+ increases from 0 to 90 (figure 10).
Low-speed streaks	The averaged spanwise wavelength is $\sim\lambda_z^+ = 100$ with a most probable wavelength of $\lambda_z^+ = 80$ (Asai *et al.* 2002).	The spanwise spacing of $NWCS_{13}$ is $D_z^+ = 110$ in the near-wall region (§ 4).
	The width of the near-wall streaks is ∼100 wall units (Kim *et al.* 1971).	
	The experimental results suggested that the lateral spacing of streaks λ^+ increases with the wall distance (Smith & Metzler 1983).	
	The DNS data presented that the lateral spacing of streaks λ^+ increases with the wall distance (Kim *et al.* 1987).	
Spanwise vorticity	The internal shear layers are formed away from the wall with slope ∼30°, generated by ejections and low-speed streaks (Schoppa & Hussain 2002).	The VVCS associated with the spanwise vorticity,$ASCS_{13}$, is inclined with 11.5° (figure 7).
	The authors found a $+\omega_3$ eddy above the probe and a $-\omega_3$ eddy below the probe (Klewicki *et al.* 1994).	For $y_r^+ > 80$, $ASCS_{13}$ presents two structures: one with positive sign above and the other with negative sign below the reference point (figure 11).
The hairpin-packet or vortex clusters	The inclination angle for the upstream envelope of the composite vortical packet is 10°. The hairpin vortices are shorter than the low-speed streaks (Zhou *et al.* 1999).	The inclination angles for $ASCS_{11}$ and $ASCS_{13}$ are less than 14° (figure 7).
	The most probable growth angle of vortex packets is $\theta \sim 12°$ (Adrian *et al.* 2000).	
	The packet of a series of vortices has an inclination angle of 12–13° from the wall (Christensen & Adrian 2001).	
	The angle of the *ramp* is ∼18° by maximum correlation of the velocity fluctuations (Brown & Thomas 1977).	The maximum inclination angle is 14° for $ASCS_{11}$ and 11.5° for $ASCS_{13}$ (figure 7).
	The angle of the clusters of the hairpins is ∼20° (Head & Bandyopadhyay 1981).	
Wall-normal vorticity structure	The most probable angle of the large-scale motions was found to be 18° by measuring the correlation of the wall shear stress and the streamwise velocity (Brown & Thomas 1977).	$ASCS_{12}$ reaches its maxima of 14° at $y_s^+ = 60$ (figure 7).
	The interface of the boundary layer is inclined at angle 20° observed in visualizations (Head & Bandyopadhyay 1981).	

TABLE 1. Detailed comparison of the characteristics of CS between the conventional CS study and the present VVCS.

Downloaded from https://www.cambridge.org/core. Open University Library, on 22 Jan 2020 at 22:43:52, subject to the Cambridge Core terms of use, available at https://www.cambridge.org/core/terms. https://doi.org/10.1017/jfm.2014.3

Acknowledgements

This work is supported by the NNSF (grant numbers 11172006, 10572004 and 90716008) and by MOST 973 project 2009CB724100. The authors would like to thank Professor Xin-Liang Li of Chinese Academy of Sciences, and thank the Shanghai Supercomputer Center.

REFERENCES

ADRIAN, R. J., MEINHART, C. D. & TOMKINS, C. D. 2000 Vortex organization in the outer region of the turbulent boundary layer. *J. Fluid Mech.* **422**, 1–54.

ADRIAN, R. J. & MOIN, P. 1988 Stochastic estimation of organized turbulent structure: homogeneous shear flow. *J. Fluid Mech.* **190**, 531–559.

ANTONIA, R. A. 1981 Conditional sampling in turbulence measurement. *Annu. Rev. Fluid Mech.* **13**, 131–156.

ANTONIA, R. A. & KIM, J. 1994 Low-Reynolds-number effects on near-wall turbulence. *J. Fluid Mech.* **276**, 61–80.

ASAI, M., MINAGAWA, M. & NISHIOKA, M. 2002 The instability and breakdown of a near-wall low-speed streak. *J. Fluid Mech.* **455**, 289–314.

BERKOOZ, G., HOLMES, P. & LUMLEY, J. N. 1993 The proper orthogonal decomposition in the analysis of turbuient flows. *Annu. Rev. Fluid Mech.* **25**, 539–575.

BROOKE, J. W. & HANRATTY, T. J. 1993 Origin of turbulenceproducing eddies in a channel flow. *Phys. Fluids A* **5**, 1011–1022.

BROWN, G. L. & THOMAS, A. S. W. 1977 Large structure in a turbulent boundary layer. *Phys. Fluids* **20** (10), S243–S252.

CHEN, J., PEI, J., SHE, Z. S. & HUSSAIN, F. 2011 Velocity–vorticity correlation structure in turbulent channel flow. *AIP Conf. Proc.* **1376** (1), 87–89.

CHRISTENSEN, K. T. & ADRIAN, R. J. 2001 Statistical evidence of hairpin vortex packets in wall turbulence. *J. Fluid Mech.* **431**, 433–443.

ECKELMANN, H., NYCHAS, S. G., BRODKEY, R. S. & WALLACE, J. M. 1977 Vorticity and turbulence production in pattern recognized turbulent flow structures. *Phys. Fluids* **20** (10), S225–S231.

FLORES, O. & JIMÉNEZ, J. 2006 Effect of wall-boundary disturbances on turbulent channel flows. *J. Fluid Mech.* **566**, 357–376.

HE, L., YI, S.-H., ZHAO, Y.-X., TIAN, L.-F. & CHEN, Z. 2011 Experimental study of a supersonic turbulent boundary layer using PIV. *Sci. China G: Phys., Mech., Astron.* **54** (9), 1702–1709.

HEAD, M. R. & BANDYOPADHYAY, P. 1981 New aspects of turbulent boundary-layer structure. *J. Fluid Mech.* **107** (1981), 297–338.

HUANG, Z.-F., ZHOU, H. & LUO, J.-S. 2007 The investigation of coherent structures in the wall region of a supersonic turbulent boundary layer based on DNS database. *Sci. China G: Phys., Mech., Astron.* **50** (3), 348–356.

HUSSAIN, A. K. M. F. & HAYAKAWA, M. 1987 Eduction of large-scale organized structures in a turbulent plane wake. *J. Fluid Mech.* **180**, 193–229.

HUSSAIN, A. K. M. F. & REYNOLDS, W.C. Measurements in fully developed turbulent channel flow. *ASME J. Fluids Engng* **97**, 568–578.

JEONG, J. & HUSSAIN, F. 1995 On the identification of a vortex. *J. Fluid Mech.* **285**, 69–94.

JEONG, J., HUSSAIN, F., SCHOPPA, W. & KIM, J. 1997 Coherent structures near the wall in a turbulent channel flow. *J. Fluid Mech.* **332**, 185–214.

KIM, H. T., KLINE, S. J. & REYNOLDS, W. C. 1971 The production of turbulence near a smooth wall in turbulent boundary layer. *J. Fluid Mech.* **50** (1), 133–160.

KIM, J., MOIN, P. & MOSER, R. 1987 Turbulence statistics in fully developed channel flow at low Reynolds number. *J. Fluid Mech.* **177**, 133–166.

KLEWICKI, J. C. & FALCO, R. E. 1996 Spanwise vorticity structure in turbulent boundary layers. *Intl J. Heat Fluid Flow* **17**, 363–376.

Downloaded from https://www.cambridge.org/core. Open University Library, on 22 Jan 2020 at 22:43:52, subject to the Cambridge Core terms of use, available at https://www.cambridge.org/core/terms. https://doi.org/10.1017/jfm.2014.3

KLEWICKI, J. C., MURRAY, J. A. & FALCO, R. E. 1994 Vortical motion contributions to stress transport in turbulent boundary layers. *Phys. Fluids* **6** (1), 277–286.

KLINE, S. J., REYNOLDS, W. C., SCHRAUB, F. A. & RUNSTADLER, P. W. 1967 The structure of turbulent boundary layers. *J. Fluid Mech.* **30**, 741–773.

KREPLIN, H.-P. & ECKELMANN, H. 1979 Propagation of perturbations in the viscous sublayer and adjacent wall region. *J. Fluid Mech.* **95** (2), 305–322.

KROGSTAD, P.-Å. & ANTONIA, R. A. 1994 Structure of turbulent boundary layers on smooth and rough walls. *J. Fluid Mech.* **277**, 1–21.

LI, X., MA, Y. & FU, D. 2001 Dns and scaling law analysis of compressible turbulent channel flow. *Sci. China Maths* **44** (5), 645–654.

LO, S. H., VOKE, P. R. & ROCKLIFE, N. J. 2000 Eddy structures in a simulated low Reynolds number turbulent boundary layer. *Flow Turbul. Combust.* **64**, 1–28.

PAN, C., WANG, J.-J. & ZHANG, C. 2009 Identification of Lagrangian coherent structures in the turbuIent boundary layer. *Sci. China* G*: Phys., Mech., Astron.* **52** (2), 248–257.

PEI, J., CHEN, J., FAZLE, H. & SHE, Z. 2013 New scaling for compressible wall turbulence. *Sci. China* G *Phys., Mech., Astron.* 1–12.

PEI, J., CHEN, J., SHE, Z.-S. & HUSSAIN, F. 2012 Model for propagation speed in turbulent channel flows. *Phys. Rev.* E **86**, 046307.

RAJAGOPALAN, S. & ANTONIA, R. A. 1979 Some properties of the large structure in fully developed turbuient duct flow. *Phys. Fluids* **22** (4), 614–622.

SCHOPPA, W. & HUSSAIN, F. 2002 Coherent structure generation in near-wall turbulence. *J. Fluid Mech.* **453**, 57–108.

SHADDEN, S. C., DABIRI, J. O. & MARSDEN, J. E. 2006 Lagrangian analysis of fluid transport in empirical vortex ring flows. *Phys. Fluids* **18** (4), 047105.

SHE, Z. S., CHEN, X., WU, Y. & HUSSAIN, F. 2010 New perspective in statistical modeling of wall-bounded turbulence. *Acta Mechanica Sin.* **26**, 847–861.

SMITH, C. R. & METZLER, S. P. 1983 The characteristics of low-speed streaks in the near-wall region of a turbulent boundary layer. *J. Fluid Mech.* **129**, 27–54.

TOMKINS, C. D. & ADRIAN, R. J. 2003 Spanwise structure and scale growth in turbulent boundary layers. *J. Fluid Mech.* **490**, 37–74.

TOWNSEND, A. A. 1970 Entrainment and the structrue of turulent flow. *J. Fluid Mech.* **41**, 13–46.

WALLACE, J. M. 2009 Twenty years of experimental and direct numerical simulation access to the velocity gradient tensor: what have we learned about turbulence?. *Phys. Fluids* **21**, 021301.

WALLACE, J. W., ECKELMANN, H. & BRODKEY, R. S. 1972 The wall region in turbulent shear flow. *J. Fluid Mech.* **54** (1), 39–48.

WILLMARTH, W. & LU, S. S. 1972 Structure of the Reynolds stress near the wall. *J. Fluid Mech.* **55** (1), 65–92.

WU, Y., CHEN, X., SHE, Z.-S. & HUSSAIN, F. 2012 Incorporating boundary constraints to predict mean velocities in turbulent channel flow. *Sci. China* G*: Phys., Mech., Astron.* **55** (9), 1691–1695.

YANG, S.-Q. & JIANG, N. 2012 Tomographic TR-PIV measurement of coherent structure spatial topology utilizing an improved quadrant splitting method. *Sci. China* G*: Phys., Mech., Astron.* **55** (10), 1863–1872.

ZHOU, J., ADRIAN, R. J., BALACHANDAR, S. & KENDALL, T. M. 1999 Mechanisms for generating coherent packets of hairpin vortices in channel flow. *J. Fluid Mech.* **387**, 353–396.

Downloaded from https://www.cambridge.org/core. Open University Library, on 22 Jan 2020 at 22:43:52, subject to the Cambridge Core terms of use, available at https://www.cambridge.org/core/terms. https://doi.org/10.1017/jfm.2014.3